



Two-dimensional and tubular structures of misfit compounds: Structural and electronic properties

Tommy Lorenz^{*1,2}, Jan-Ole Joswig¹ and Gotthard Seifert¹

Review

Open Access

Address:

¹Theoretische Chemie, Technische Universität Dresden, 01069 Dresden, Germany and ²Helmholtz-Zentrum Dresden-Rossendorf e.V., Institute of Ion Beam Physics and Materials Research, P.O. Box 51 01 19, 01314 Dresden, Germany

Email:

Tommy Lorenz* - tommy.lorenz@chemie.tu-dresden.de

* Corresponding author

Keywords:

2D layered materials; misfit layer compounds

Beilstein J. Nanotechnol. **2014**, *5*, 2171–2178.

doi:10.3762/bjnano.5.226

Received: 28 July 2014

Accepted: 30 October 2014

Published: 19 November 2014

This article is part of the Thematic Series "Atomic scale interface design and characterisation: Theory – Electronic properties".

Guest Editor: A. Krashennikov

© 2014 Lorenz et al; licensee Beilstein-Institut.

License and terms: see end of document.

Abstract

Misfit layer compounds are structures that consist of two sublattices differing in at least one of their lattice constants. The two different layers are stacked either an alternating or in a more complex series resulting in mono- or multi-layer misfit compounds. To date, planar and bent misfit structures, such as tubes, scrolls or nanoparticles, have been synthesized and interesting magnetic and physical properties have been observed as a result of their special structures. Based on these observations, we present an overview of such misfit systems and summarize and discuss their electronic structure as well as the interlayer bonding behaviour, which is not completely understood yet. Furthermore, a more detailed insight into the SnS–SnS₂ system is given, which was the first tubular misfit compound that has been synthesized and extensively investigated.

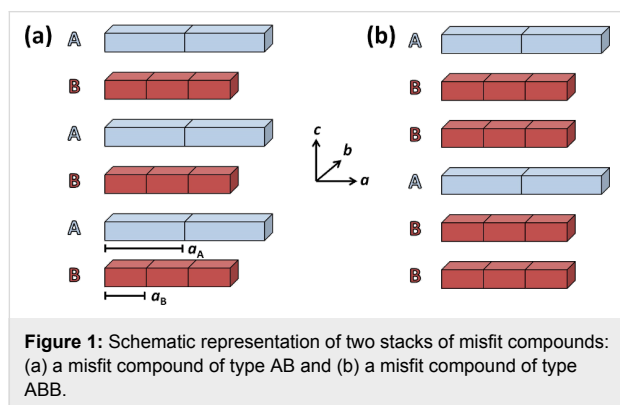
Review

Introduction

Sheets of different two-dimensional, layered materials can assemble to form composite materials. As the compounds usually exhibit their own symmetry and space groups, their unit cells differ in most cases in either one, two, or all three directions. The combination of any two or more layers of these sheets results in a so-called misfit layer compound (MLC) [1,2], in which the difference in the compound layers leads to different effects. Figure 1a demonstrates the misfit-compound

concept schematically: two different layered, 2D materials are stacked alternately in different sequences. These materials exhibit the stoichiometries MX and TMX₂, and their total chemical formula is (MX)_{1+x}(TMX₂)_m (with M = Sn, Pb, Bi, Sb, rare earths; TM = Ti, V, Cr, Nb, Ta; X = S, Se, 0.08 < x < 0.28, m = 1–3) [3]. The unit cell parameters are dissimilar at least in one direction (crystallographic direction *a* in Figure 1). The review by Meerschaut [4] considered misfit compounds with

different unit cell lengths in one direction (a) only. Additionally, compounds that are different in both in-plane directions (a and b) are also known. For example, $(\text{SnS})_{1.32}\text{SnS}_2$, $(\text{PbSe})_{0.99}\text{WSe}_2$, $(\text{PbSe})_{1.00}\text{MoSe}_2$, and $(\text{SnSe})_{1.03}\text{MoSe}_2$ [5–8], and misfit layer compounds consisting of other elements such as tellurium [9] or lanthanides [10] have been synthesized. Although some misfit compounds occur naturally [1,11], the recent developments in the synthesis, exfoliation, and handling of layered, two-dimensional (2D) materials gave access to the preparation of numerous misfit compounds.

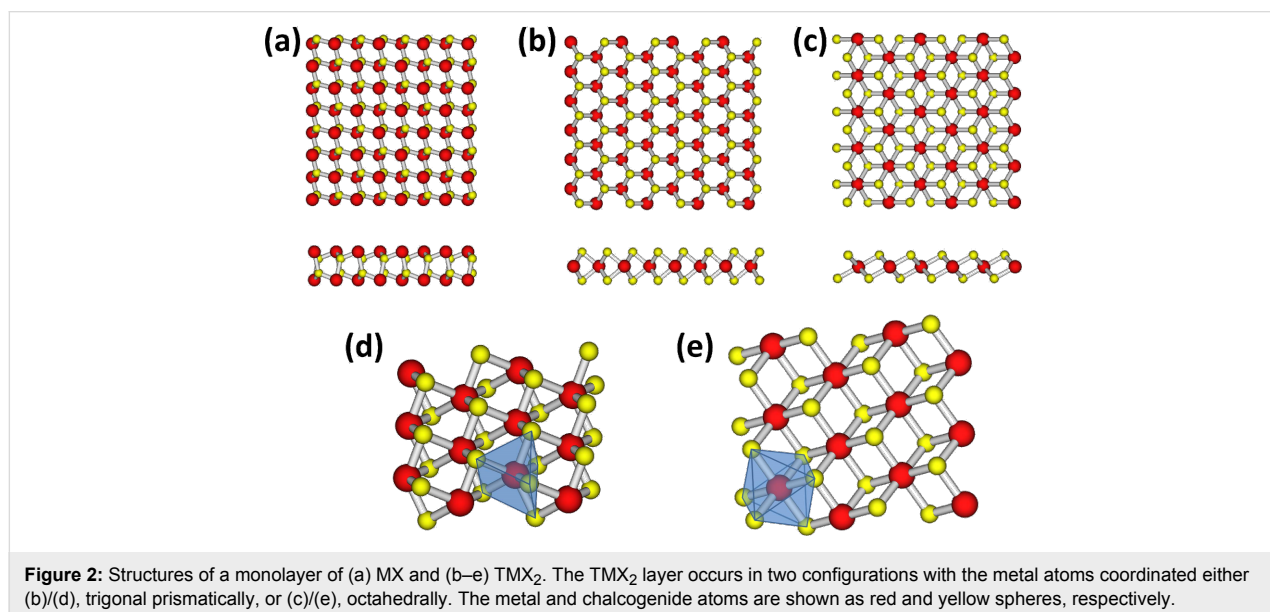


To date, three comprehensive reviews have dealt with planar [3,4] and tubular [6] misfit compounds, which were as well the foundation for the present overview. In the following, planar and tubular misfit structures are discerned and their individual structural and electronic properties are discussed. Note that the following sections are sorted with respect to the reviewed properties. A section containing special examples will be followed by a summary.

Structures

Layered chalcogenides most commonly form misfit compounds [3] with stoichiometries MX/TMX_2 (chemical formula $(\text{MX})_{1+y}(\text{TMX}_2)_m$ with $\text{M} = \text{Sn, Pb, Bi, Sb, rare earths}$; $\text{TM} = \text{Ti, V, Cr, Nb, Ta}$; $\text{X} = \text{S, Se}$, $0.08 < y < 0.28$, $m = 1-3$). The lengths of the lattice vectors \vec{a}_1 and \vec{a}_2 (the indices label the two components of the misfit compound) in the mismatched direction determine the ratio of MX to $(\text{TMX}_2)_m$. This is expressed in the sum formula by the variable y and can be derived as $y = (4/2) \cdot (a_2/a_1) - 1$. The individual layer types, that is, MX and TMX_2 , have different stoichiometries, and thus, differing structures. Whereas MX layers show a distorted rock salt structure (Figure 2a), the TMX_2 layers have a sandwich structure, where a sheet of (transition) metal atoms is sandwiched by two layers of chalcogenide atoms (Figure 2b,c). The transition metal atoms can assemble in a trigonal prismatic or octahedral coordination in the TMX_2 layer (Figure 2d,e). The TMX_2 labeling is according to the polytypes of their lamellar compounds, that is, their stacking order (number of layers in the unit cell) and symmetry (T, H, R for trigonal, hexagonal, rhombohedral symmetry, respectively) generate the labels.

As can be seen in Figure 1, different sequences of stacking are possible: Either an alternating A–B–A–B–... stacking (Figure 1a) or bi- ($m = 2$) and trilayer ($m = 3$) systems are known. Here, the parameter m indicates the number of successive layers of the same type. In the latter two cases, two or three TMX_2 layers follow directly and are embedded into two MX layers as shown in Figure 1b. In these cases, the TMX_2 layers are held together by van der Waals forces, whereas the interaction between MX and TMX_2 layers is based on van der Waals interaction and a charge transfer (CT) from MX to TMX_2 [12].



Thus, misfit compounds do not only differ by stoichiometry, difference in structure, and individual coordination in the TMX_2 layer, but also by the ratio between the two subsystems, MX and TMX_2 .

Planar structures

We will now focus on a discussion of crystallographic data obtained from different planar misfit compounds. In most cases, the angle between the in-plane lattice vectors \vec{a} and \vec{b} (as defined in Figure 1) is 90° , so that the \vec{a} and \vec{b} vectors in both interacting compounds are parallel. If the \vec{b} vectors have the same length, $\vec{b}_1 = \vec{b}_2$ results. An exception is reported by Ren et al. [13] for $(\text{SbS})_{1.15}\text{TiS}_2$ with angles of $\gamma_1 = 84.06^\circ$ and $\gamma_2 = 90.01^\circ$. Generally, the differences occur regularly in both directions as a result of right-angled in-plane lattice vectors.

Most of the systems with NbX_2 or TaX_2 sublayers in a trigonal prismatic coordination have α angles of nearly 90° . There are, however, misfit compounds with different \vec{c} vectors and α or β angles deviating from 90° , for example, $(\text{YS})_{1.23}\text{NbS}_2$ [14] and $(\text{HoS})_{1.23}\text{NbS}_2$ [15] with trigonal prismatic TMX_2 layers, monoclinic $(\text{PbS})_{1.18}\text{TiS}_2$ [16] and $(\text{PbS})_{1.12}\text{VS}_2$ [17], or triclinic $(\text{LaS})_{1.20}\text{CrS}_2$ [18] and $(\text{SnS})_{1.20}\text{TiS}_2$ [19], all four with octahedral coordination in the TMX_2 layer. The unit cell parameters of some misfit compounds are given in Table 1.

As mentioned above, different types of stacking are possible for these composite structures. They may differ, for example, in the

number of sub-layers, their symmetry and orientation. The most common structures are $2H$ and $3R$. Due to the weak interlayer forces, layer exfoliation is easily possible [24].

As a consequence of their structure, interaction between the M atoms of the MX layer and the X atoms of the TMX_2 layer exists in all misfit compounds. In each unit cell this interaction occurs twice: at the top and the bottom sides of the layers. This can be seen in Figure 3. Additionally, this figure shows that the symmetry of the misfit compound's unit cell is determined by the sublayers and their symmetries. The metal atoms of the TMX_2 sublayer can be coordinated trigonally prismatic by the chalcogenide atoms (Figure 3a), so that the symmetry of the whole cell is orthorhombic as, for example, in $(\text{SnS})_{1.17}\text{NbS}_2$. On the other hand, for a monoclinic misfit compound such as $(\text{PbS})_{1.18}\text{TiS}_2$, the TMX_2 sublayers have a (distorted) octahedral symmetry (Figure 3b).

In cases where the misfit occurs in only one direction, for example, in b , the number of stacking possibilities grows, since the individual layers may be centered differently with respect to the b direction (see Figure 4). Each subsystem has either a so-called C-centered or an F-centered lattice. In both cases, the c axes match. In the F-centered structure, the length of the c axis in the unit cell is doubled due to an additional shift of $1/2c$. Accordingly, four different possibilities of stacking are possible: CC, CF, FC, and FF (see Figure 4). In the CC system, the two c axes of the subsystems completely match (in direc-

Table 1: Cell parameters of different misfit layer compounds. This table has been taken from Rouxel et al. [3].

Compound	a_1 [Å]	a_2 [Å]	$y = 2 \cdot (a_2/a_1) - 1$	$b_1 = b_2$ [Å]	$c_1 = c_2$ [Å]	α [deg.]	Ref.
$(\text{SnS})_{1.17}\text{NbS}_2$	5.673	3.321	0.1708	5.751	11.761	90	[20,21]
$(\text{LaS})_{1.14}\text{NbS}_2$	5.828	3.310	0.1359	5.797	$c_1 = 11.52^a$ $c_2 = 23.94$	90	[22,23]
$(\text{PbS})_{1.18}\text{TiS}_2$	5.800	3.409	0.1755	5.881	11.76	95.28	[16]

^a $c_2 = 2c_1$.

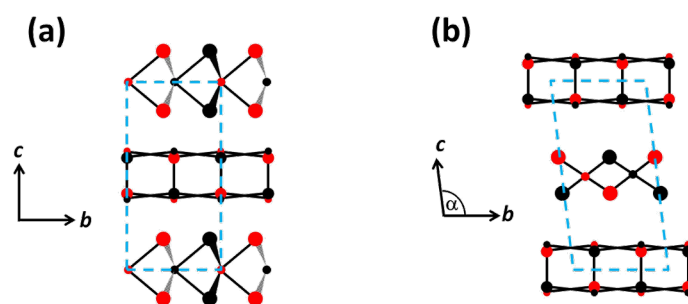


Figure 3: Side view of two unit cells of misfit layer compounds with the TMX_2 component either in trigonal prismatic (a) or octahedral coordination (b). The unit cells are denoted by the blue boxes. Adapted with permission from [3]. Copyright 1995 Elsevier.

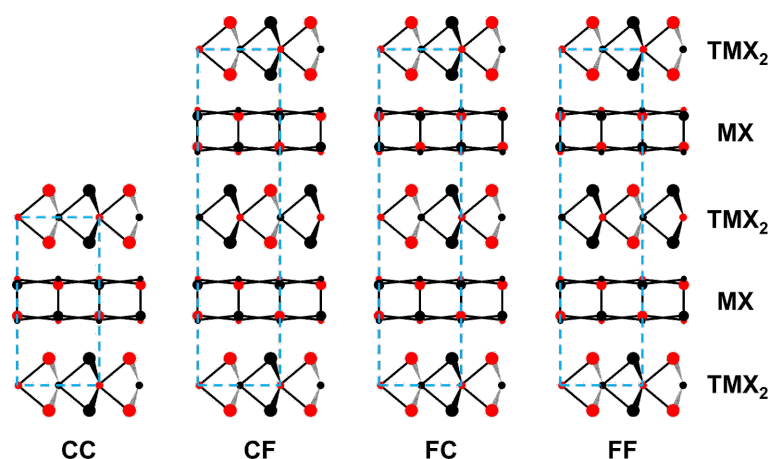


Figure 4: Different possible stacking types of misfit compounds projected along the [100] direction. The blue boxes denote the unit cell and the colored circles represent the metal (small circles) and chalcogenide atoms (large circles), where the different colors represent the different positions in space: black atoms above the paper-plane and red ones beneath it. Adapted with permission from [3]. Copyright 1995 Elsevier.

tion and length) which is the case, for example, in the compound $(\text{SnS})_{1.17}\text{NbS}_2$. In the FC system, $c_1 = 2 \cdot c_2$ as it occurs in, for example, $(\text{YS})_{1.23}\text{NbS}_2$, whereas $c_2 = 2 \cdot c_1$ is seen in CF systems such as $(\text{LaS})_{1.14}\text{NbS}_2$. In misfit compounds of the FF type, both \vec{c} vectors have the same direction and norm, but twice the length as the CC type. The structure of $(\text{PbS})_{1.13}\text{TaS}_2$ is an example of the latter type.

Non-planar structures

In addition to the previously discussed planar misfit structures, bent systems are common as well [5,6,25–29]. Such tubular or cylindrical misfit layer compounds have been mentioned for the first time in relation to the mineral cylindrite [1,30]. Generally, it is assumed that a misfit in a and b directions leads to the formation of tubular structures by reason of energy minimizing [6]. The advantage of these structures is the absence of any dangling bonds, which leads to more energetically stable systems compared to the finite planar ones (stripes, flakes, platelets) [31,32]. Hence, the act of bending or rolling can be seen as a relaxation process, although the relative thickness of the tube walls and the rigidity of the interatomic bonds were seen as a steric hindrance. The rolling process has been discussed in relation to the misfit compounds $(\text{PbS})_{1.14}(\text{NbS}_2)_2$ [29], $(\text{BiS})_{1.17}(\text{NbS}_2)_n$ [33] with $n = 1–4$ or $(\text{SnS})_{1.32}\text{SnS}_2$ [25]. Just as for planar misfit compounds, different stacking types are possible in the bent misfit systems as well regarding the number of sublayers, or rather, the stacking order (as shown in Figure 1), and also regarding the possibility of different structures and orientations of the sublayers, as shown in Figure 3 and Figure 4. For example, several different stacking configurations have been observed for $(\text{SnS})_{1.32}(\text{SnS}_2)_n$, such as ABAB, ABBABB, ABABBABABB [6,26]. As in planar misfit systems, the composite has a global super-symmetry that may

differ from that of the two subsystems. Due to two different lattice vectors (\vec{a} and \vec{b}), multiple in-plane orientations of the sublayers are possible, which leads to different rolling vectors and therefore, to a manifold of chiral nanotubes. However, aside from tubular misfit layer compounds, nanoscrolls and nanoparticles containing sublayers with different lattices were produced [5,6,25,26], which can have the same structural parameters (stacking order, number and orientation of sublayers, etc.) as tubes and planar misfit compounds.

Electronic structure and interlayer bonding

Meerschaut [4] suggests that the properties of misfit layer compounds might be attributed to the properties of the individual compounds or subsystems. For example, the van der Waals gap in TMX_2 systems can be chemically intercalated [34]. A misfit compound can, thus, be viewed as a TMX_2 system intercalated by another layered MX system. As a consequence, the electronic properties of some misfit compounds have been successfully described by a rigid-band formalism. In this description, the electronic bands are taken as immutable characteristics and only the filling is changed depending on the intercalated species.

In addition to theoretical considerations, the electronic structure is discernible by spectroscopy as Ohno [12,35] presented in 1991. By performing X-ray photoelectron and absorption spectroscopy (XPS, XAS) and reflection electron energy loss spectroscopy (REELS), it was revealed that the electronic structure indeed can be well-described by a superposition of bands of individual single layers. From these results it was concluded that a charge transfer from MX to TMX_2 takes place, which is independent from the nature of the metal M (either M^{2+} : Sn, Pb, or M^{3+} : La, Ce, Sm). In that case, MX can be viewed as a donor

and TMX_2 as an acceptor of the transferred electron density. This claim was based on studies of valence band XPS and XAS spectra of the misfit compounds, compared to those of the individual layers, and a spectrum of iron intercalated titanium disulfide ($\text{Fe}_{1/3}\text{TiS}_2$), which can be interpreted as a true intercalated system. Figure 5 in [35] shows this XAS spectra of the K absorption edge of sulfur for the systems TiS_2 , PbS , PbTiS_3 (=MLC $(\text{PbS})_{1.18}\text{TiS}_2$), and $\text{Fe}_{1/3}\text{TiS}_2$. The shapes of the PbTiS_3 and $\text{Fe}_{1/3}\text{TiS}_2$ spectra are quite similar. From this, charge transfer was concluded, which should result from the filling of the t_{2g} energy levels coming from the titanium d states.

Further studies used a comparable argument for the claim of charge transfer in other misfit layer compounds. One example is the electron transfer from PbSe to NbSe_2 in $[(\text{PbSe})_{1.14}]_m(\text{NbS}_2)_1$ with $m = 1-6$ [36]. The electronic structure has been predicted by density functional theory calculations using the generalized gradient approximation. From the overlap of the empty bands in NbS_2 with the filled valence band of PbSe , the authors concluded that “only a small fraction of an electron’s charge is transferred per atom” [36]. In Figure 5 the density of states of the electronic bands of PbSe and NbSe_2 near the Fermi level are displayed schematically. The overlap of the $\text{Se}(\text{PbSe})$ 4p states with the $\text{Nb } d_{z^2}$ states can be seen clearly, which is used as an argument for potential charge transfer. Additionally, the dependence on the number of PbSe sublayers in one unit cell of the misfit compound has been investigated (varying m in the sum formula) with the result that the interlayer charge transfer increases with increasing m .

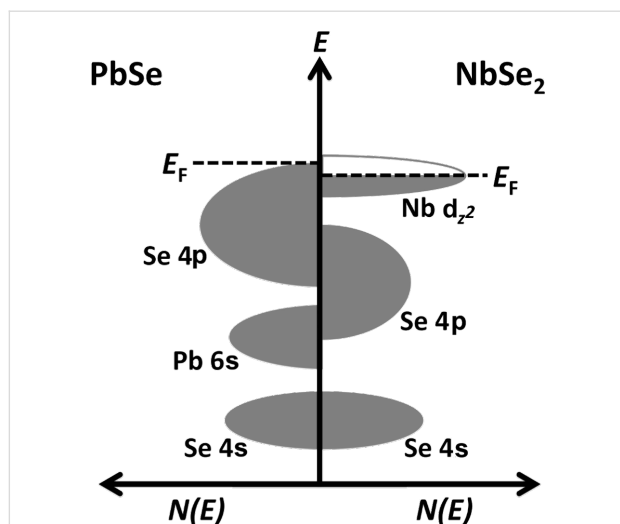


Figure 5: Schematic representation of the density of states of a PbSe layer (left) and a NbSe_2 layer (right). The electron transfer takes place from the PbSe valence band to the conduction band of the NbSe_2 layer. Adapted with permission from [36]. Copyright 2014 American Chemical Society.

Another theoretical work [37] analysed the band structure of $(\text{SnS})_{1.17}\text{NbS}_2$ by using a ratio of \bar{a} vectors of 5:3 resulting in a $(\text{SnS})_{1.20}\text{NbS}_2$ stoichiometry. The authors concluded a charge transfer of 0.4 electrons per niobium atom from their calculations. Furthermore, they showed that the $\text{Sn } 5s$ orbitals mix strongly with the $\text{S } 3p$ orbitals from NbS_2 .

Moreover, vibrational spectroscopy has been used to investigate a possible interlayer charge transfer. The Raman spectra of $(\text{SnS})_{1.17}\text{NbS}_2$ and $(\text{PbS})_{1.18}\text{TiS}_2$ (powdered samples and single crystals) as well as single crystals of $(\text{PbS})_{1.14}\text{NbS}_2$ were compared to those of the pure substances and showed a superposition of the interlayer vibrations of the individual layers. Shifts in the NbS_2 modes relative to those in 2H-NbS_2 were interpreted to be a result of charge transfer. These spectra are published in [38,39].

In contrast to the previously shown examples, Ettema and Haas [40] performed XPS measurements for the core states of misfit layer compounds. This work can be seen as an extension of Ohno’s work [12,35], which was limited to the valence bands and has been discussed above. They showed that tin and lead are divalent in compounds of the structure $(\text{MX})_{1+y}\text{TMX}_2$ due to the fact that the core-level binding energies of these elements do not differ in either the misfit compounds or the isolates systems (SnS , PbS). If a (small) charge transfer took place, the core-level energies of the TM atoms in the TMS_2 sublayer would have stayed nearly constant. Experimentally, this shift in binding energy was not observed for the $2s$, $2p$, $3s$, $3p$ levels of Ti , the $3s$, $3p$, $3d$, $4s$, $4p$ levels of Nb and the $4p$, $4d$, $5p$, and $4f$ levels of Ta . From this fact, the authors concluded that there is no significant interlayer charge transfer and the stability of the misfit layer compounds results from covalent bonds between the several sublayers.

Mořlo et al. [41] investigated different misfit systems consisting of Sn and Pb (single-, double- and triple-layer, i.e., $m = 1-3$) using electron microprobe analysis. Since the M and TM atoms are in oxidation states +2 and +4, respectively, each sublayer should be uncharged and electronically balanced. Hall and Seebeck measurements performed by Auriel et al. [42] showed a highly anisotropic metallic behaviour of misfit layer compounds; some of them even showed a transition to superconductivity at temperatures less than 6 K. A small intrinsic charge transfer could explain such physical properties. However, it is quite improbable that (especially) lead has oxidation states higher than +2 in a Pb-S system. Thus, a charge transfer from $\text{Pb}(\text{MX})$ to TMX_2 is unlikely. The concept of cationic coupling assumes an M (e.g., Pb or Sn) deficiency in the MX layer and therefore a TM (e.g., Nb) excess. In fact, some of the M^{2+} cations in the MX sublayer are substituted by

TM^{3+} ions. The excess of positive charge must then be adjusted by reduction of the same amount of TM^{4+} ions in the TMX_2 layer. Thus, the MX sublayer is positively charged and, as a consequence, the TMX_2 layer becomes negative, so that a charge transfer is introduced. The resulting strong, attractive, electrostatic interaction between the two sublayers is the origin of the stability of the misfit compounds within the concept of cationic coupling.

To conclude this section, we will briefly mention the so-called graphite intercalation compounds (GICs) [43] that consist of several graphene layers, which are intercalated by different atoms or fragments, for example, alkali and alkaline earth derivatives or metal halide derivatives. Those components are held together by charge transfer and not every van der Waals gap is intercalated by guest atoms. The systems are called “stage 1 compounds” in the case of an alternating arrangement, and “stage 2 compounds”, if every second graphene layer is intercalated, and so on. In contrast to misfit structures, which were the focus of this review, the host molecules and atoms in GICs are intercalated and do not have the same or comparable lattice structure as they have in their bulk phases. For this reason we will not go beyond mentioning GICs here and refer the interested reader to the respective literature.

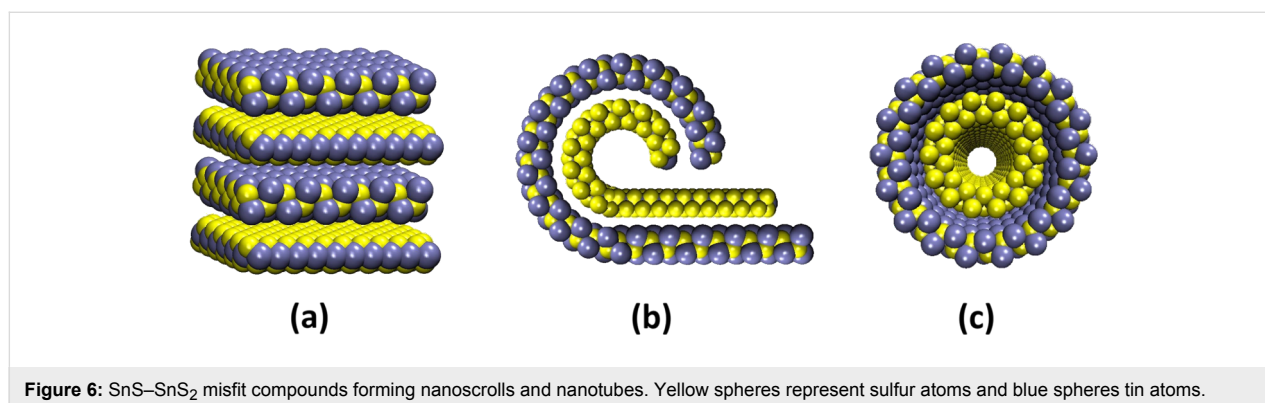
Examples

SnS–SnS₂ layers and nanotubes

In 2003, inorganic fullerene-like nanoparticles and small nanotubes were synthesized [5]. These structures have spherical or polyhedral shapes and consist of orthorhombic SnS and hexagonal SnS₂ lattices. The two sublattices have the same structure and orientation as the “classical” layered misfit compounds discussed above. Meanwhile, SnS–SnS₂ nanostructures have been further produced, such as nanotubes and nanoscrolls (see Figure 6). These structures have been extensively experimentally and theoretically investigated to date [6,25,26,44]. Selected area electron diffraction (SAED) measurements showed that the interlayer distance between the SnS and SnS₂

substructures is nearly unchanged relative to the bulk structures (error 3%) [26]. For this reason, it is estimated that the sublattice structures in the SnS–SnS₂ system are almost the same as in the pristine bulk material. As a consequence, both in-plane directions are different from one another. The resulting SnS–SnS₂ nanotubes result in the stoichiometries $(\text{SnS})_{1.32}\text{SnS}_2$, $(\text{SnS})_{1.32}(\text{SnS}_2)_2$ and $[(\text{SnS})_{1.32}]_2(\text{SnS}_2)_3$. SAED patterns further show that the SnS₂ subsystems in these misfit tubes have two different rolling directions. This is equivalent to two different SnS₂ chiralities (zig-zag, armchair tubes) in the misfit tube.

A recent theoretical study performed with density functional-based tight-binding calculations investigated a possible charge transfer between the SnS and SnS₂ layers. By comparing the density of states (DOS) for a hypothetical SnS–SnS₂ misfit system with the sum of the DOSs of the two isolated monolayers, the authors showed that additional states arise in the gap region hinting at an electronic interaction between the layers. Furthermore, the atomic charges in the combined system obtained by Mulliken population analysis surprisingly showed that the SnS₂ layer was slightly positively charged, whereas the SnS layer was negatively charged. Although the received charge transfer is quite small (approx. 0.1 electrons per SnS₂ unit) the direction of the electron transfer was perplexing, especially because this direction is unexpected because the Sn^{4+} system transfers electron density to the Sn^{2+} system. The explanation might be that the charge transfer does not take place from metal to metal ($\text{Sn}^{2+} \rightarrow \text{Sn}^{4+}$), because Sn is not a transition metal, in contrast to the TMX_2 systems discussed above. Thus, the sulfur atoms of the SnS₂ layer could act as donors and Sn^{2+} atoms in the SnS layer as acceptors. Generally, Sn^{2+} can act as an acceptor if a stronger reducer is present. By comparing the standard potentials of the S^{2-}/S and Sn/Sn^{2+} systems, it appears that this explanation is possible and is supported by the fact that in the SnS₂–SnS bilayer, only the SnS₂-sulfur atoms facing the SnS layer become slightly positive (see Figure 5 in [44]).



SiO_x-coated carbon nanotubes

In 2002, carbon–SiO_x-based nanocomposites were synthesized [27,28]. Although these structures differ significantly from the discussed misfit compounds, the two host lattices adjust and the mechanical strain is reduced by a spontaneous bending. Figure 7a shows the two planar sublattices in which the hexagonal carbon structure (graphene) and the six-membered SiO₄ rings align their lattice constants. To minimize the energy, the C–Si-bonded system bends spontaneously (Figure 7b). This relaxation process leads to the formation of tubular structures and Si–O–Si bond angles of 140°. In this system, a real covalent bond between the two subsystems can be observed, which partly changes the hybridization of the carbon atoms from sp² to sp³.

Conclusion

In this review, the structures of misfit layer compounds were discussed. As was illustrated, MLCs consist of two different sublattices with at least one lattice vector of different length in the subsystems. By aligning their lattices, the layers with stoichiometries MX and TMX₂ can be stacked alternating or in more complex sequences connecting to a misfit compound. They can adopt planar or bent structures, and the resulting super-symmetry usually differs from the symmetry of the pristine systems. To date, layers, tubes, nanoparticles, and nanorolls formed by misfit layer compounds are known and have been synthesized. In the non-alternating A–B–B–... stacking, the successive layers of the same type are bonded only by van der Waals interaction. This is one reason why it is possible to intercalate metal atoms within this van der Waals gap. Due to the fact that layered materials show exceptional lubricating properties originating in strong intra-layer, but weak inter-layer interactions, lubricating properties can be expected for misfit layer compounds as well.

For the purpose of structure determination, many measurements and experiments have been performed for misfit layer

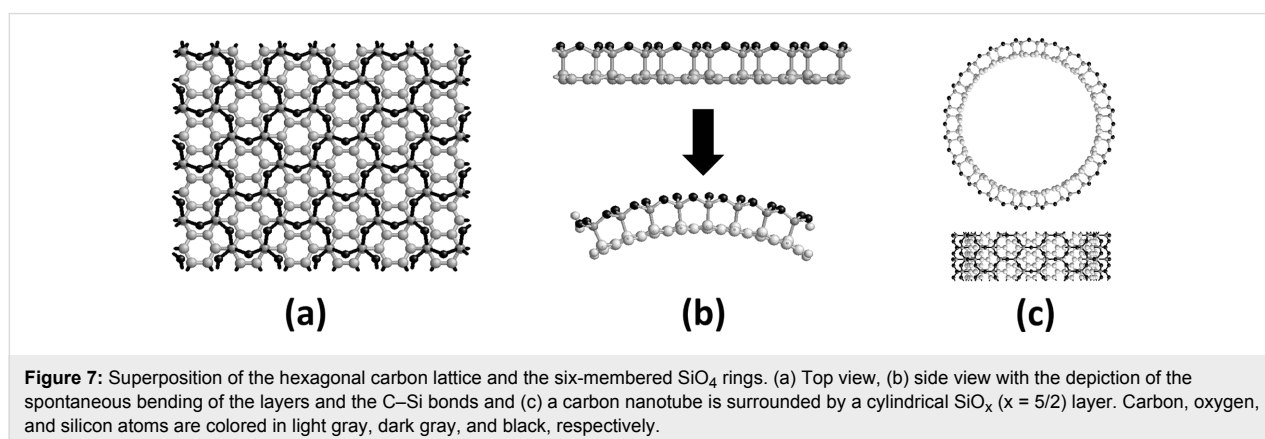
compounds. Furthermore, the determination of their electronic structure has been implemented considerably. From this data, estimations of the bonding behaviour between the sublattices were made. On the one hand, a charge transfer from the MX to the TMX₂ layer is mentioned, on the other hand the concept of cation coupling is discussed, which assumes the substitution of M²⁺ by TM³⁺ cations in the MX layer. This might introduce a charge transfer through the necessity of electroneutrality for the whole system. The presented concepts may explain the stability of the misfit layer compounds and their properties, but further studies are necessary for a comprehensive description of these interesting systems.

Acknowledgements

The authors acknowledge financial support by the European Union via ERC grant INTIF 226639 and Dr. Igor Baburin for fruitful discussions.

References

- Makovicky, E.; Hyde, B. G. Non-commensurate (misfit) layer structures. In *Inorganic Chemistry*; Mingos, D. M. P., Ed.; Structure and Bonding, Vol. 46; Springer: Berlin, Heidelberg, 1981; pp 101–170.
- Meerschaut, A., Ed. *Incommensurate Sandwiched Layered Compounds*; Trans Tech: Zürich, 1992.
- Rouxel, J.; Meerschaut, A.; Wiegers, G. A. *J. Alloys Compd.* **1995**, *229*, 144–157. doi:10.1016/0925-8388(95)01680-5
- Meerschaut, A. *Curr. Opin. Solid State Mater. Sci.* **1996**, *1*, 250–259. doi:10.1016/S1359-0286(96)80092-1
- Hong, S. Y.; Popovitz-Biro, R.; Prior, Y.; Tenne, R. *J. Am. Chem. Soc.* **2003**, *125*, 10470–10474. doi:10.1021/ja036057d
- Radovsky, G.; Popovitz-Biro, R.; Stroppa, D. G.; Houben, L.; Tenne, R. *Acc. Chem. Res.* **2014**, *47*, 406–416. doi:10.1021/ar400138h
- Smeller, M. M.; Heideman, C. L.; Lin, Q.; Beekman, M.; Anderson, M. D.; Zschack, P.; Anderson, I. M.; Johnson, D. C. *Z. Anorg. Allg. Chem.* **2012**, *638*, 2632–2639. doi:10.1002/zaac.201200408
- Lin, Q.; Smeller, M.; Heideman, C. L.; Zschack, P.; Koyano, M.; Anderson, M. D.; Kykyneshi, R.; Keszler, D. A.; Anderson, I. M.; Johnson, D. C. *Chem. Mater.* **2010**, *22*, 1002–1009. doi:10.1021/cm901952v



9. Moore, D. B.; Beekman, M.; Disch, S.; Johnson, D. C. *Angew. Chem., Int. Ed.* **2014**, *53*, 5672–5675. doi:10.1002/anie.201401022
10. Panchakarla, L. S.; Popovitz-Biro, R.; Houben, L.; Dunin-Borkowski, R. E.; Tenne, R. *Angew. Chem., Int. Ed.* **2014**, *53*, 6920–6924. doi:10.1002/anie.201404189
11. Makovicky, E.; Hyde, B. G. *Mater. Sci. Forum* **1992**, *100–101*, 1–100. doi:10.4028/www.scientific.net/MSF.100-101.1
12. Ohno, Y. *Solid State Commun.* **1991**, *79*, 1081–1084. doi:10.1016/0038-1098(91)90015-N
13. Ren, Y.; Meetsma, A.; Petricek, V.; van Smaalen, S.; Wiegers, G. *Acta Crystallogr., Sect. B: Struct. Sci.* **1995**, *51*, 275–287. doi:10.1107/S0108768194014035
14. Rabu, P.; Meerschaut, A.; Rouxel, J.; Wiegers, G. A. *J. Solid State Chem.* **1990**, *88*, 451–458. doi:10.1016/0022-4596(90)90241-O
15. Wiegers, G. A.; Meetsma, A.; Haange, R. J.; de Boer, J. L. *J. Alloys Compd.* **1992**, *178*, 369–378. doi:10.1016/0925-8388(92)90277-G
16. Van Smaalen, S.; Meetsma, A.; Wiegers, G. A.; de Boer, J. L. *Acta Crystallogr., Sect. B: Struct. Sci.* **1991**, *47*, 314–325. doi:10.1107/S0108768190013477
17. Onoda, M.; Kato, K.; Gotoh, Y.; Oosawa, Y. *Acta Crystallogr., Sect. B: Struct. Sci.* **1990**, *46*, 487–492. doi:10.1107/S0108768190003950
18. Kato, K.; Kawada, I.; Takahashi, T. *Acta Crystallogr., Sect. B: Struct. Crystallogr. Cryst. Chem.* **1977**, *33*, 3437–3443. doi:10.1107/S0567740877011157
19. Wiegers, G. A.; Meetsma, A.; de Boer, J. L.; van Smaalen, S.; Haange, R. J. *J. Phys.: Condens. Matter* **1991**, *3*, 2603–2612. doi:10.1088/0953-8984/3/16/001
20. Wiegers, G. A.; Meetsma, A.; Haange, R. J.; de Boer, J. L. *Mater. Res. Bull.* **1988**, *23*, 1551–1559. doi:10.1016/0025-5408(88)90243-7
21. van Smaalen, S. *J. Phys.: Condens. Matter* **1989**, *1*, 2791–2800. doi:10.1088/0953-8984/1/17/002
22. Meerschaut, A.; Rabu, P.; Rouxel, J.; Monceau, P.; Smontara, A. *Mater. Res. Bull.* **1990**, *25*, 855–861. doi:10.1016/0025-5408(90)90062-7
23. Wiegers, G. A.; Meetsma, A.; Haange, R. J.; van Smaalen, S.; de Boer, J. L.; Meerschaut, A.; Rabu, P.; Rouxel, J. *Acta Crystallogr., Sect. B: Struct. Sci.* **1990**, *46*, 324–332. doi:10.1107/S0108768190001252
24. Bonneau, P.; Mansot, J. L.; Rouxel, J. *Mater. Res. Bull.* **1993**, *28*, 757–766. doi:10.1016/0025-5408(93)90016-7
25. Radovsky, G.; Popovitz-Biro, R.; Staiger, M.; Gartsman, K.; Thomsen, C.; Lorenz, T.; Seifert, G.; Tenne, R. *Angew. Chem., Int. Ed.* **2011**, *50*, 12316–12320. doi:10.1002/anie.201104520
26. Radovsky, G.; Popovitz-Biro, R.; Tenne, R. *Chem. Mater.* **2012**, *24*, 3004–3015. doi:10.1021/cm301491v
27. Grobert, N.; Seeger, T.; Seifert, G.; Rühle, M. *J. Ceram. Process. Res.* **2003**, *4*, 1–5.
28. Seeger, T.; Cöhler, T.; Frauenheim, T.; Grobert, N.; Terrones, M.; Seifert, G.; Rühle, M. *Z. Metallkd.* **2002**, *93*, 455–458. doi:10.3139/146.020455
29. Bernaerts, D.; Amelinckx, S.; Van Tendeloo, G.; Van Landuyt, J. *J. Cryst. Growth* **1997**, *172*, 433–439. doi:10.1016/S0022-0248(96)00747-6
30. Williams, T. B.; Hyde, B. G. *Phys. Chem. Miner.* **1988**, *15*, 521–544. doi:10.1007/BF00311023
31. Seifert, G.; Köhler, T.; Tenne, R. *J. Phys. Chem. B* **2002**, *106*, 2497–2501. doi:10.1021/jp0131323
32. Brüser, V.; Popovitz-Biro, R.; Albu-Yaron, A.; Lorenz, T.; Seifert, G.; Tenne, R.; Zak, A. *Inorganics* **2014**, *2*, 177–190. doi:10.3390/inorganics2020177
33. Gómez-Herrero, A.; Landa-Cánovas, A. R.; Hansen, S.; Otero-Díaz, L. C. *Micron* **2000**, *31*, 587–595. doi:10.1016/S0968-4328(99)00141-9
34. Hernán, L.; Morales, J.; Pattanayak, J.; Tirado, J. L. *J. Solid State Chem.* **1992**, *100*, 262–271. doi:10.1016/0022-4596(92)90100-A
35. Ohno, Y. *Phys. Rev. B* **1991**, *44*, 1281–1291. doi:10.1103/PhysRevB.44.1281
36. Alemayehu, M. B.; Mitchson, G.; Ditto, J.; Hanken, B. E.; Asta, M.; Johnson, D. C. *Chem. Mater.* **2014**, *26*, 1859–1866. doi:10.1021/cm404018a
37. Fang, C. M.; Ettema, A. R. H. F.; Haas, C.; Wiegers, G. A.; van Leuken, H.; de Groot, R. A. *Phys. Rev. B* **1995**, *52*, 2336–2347. doi:10.1103/PhysRevB.52.2336
38. Sourisseau, C.; Cavagnat, R.; Tirado, J. L. *J. Raman Spectrosc.* **1992**, *23*, 647–651. doi:10.1002/jrs.1250231114
39. Hangyo, M.; Nakashima, S.; Hamada, Y.; Nishio, T.; Ohno, Y. *Phys. Rev. B* **1993**, *48*, 11291–11297. doi:10.1103/PhysRevB.48.11291
40. Ettema, A. R. H. F.; Haas, C. *J. Phys.: Condens. Matter* **1993**, *5*, 3817–3826. doi:10.1088/0953-8984/5/23/008
41. Moëlo, Y.; Meerschaut, A.; Rouxel, J.; Auriel, C. *Chem. Mater.* **1995**, *7*, 1759–1771. doi:10.1021/cm00058a003
42. Auriel, C.; Meerschaut, A.; Deudon, C.; Wiegers, G. A.; Baas, J.; Chen, J.; Monceau, P. *Eur. J. Solid State Inorg. Chem.* **1995**, *32*, 947–962.
43. Rüdorff, W. *Adv. Inorg. Chem. Radiochem.* **1959**, *1*, 223–266.
44. Lorenz, T.; Joswig, J.-O.; Seifert, G. *Semicond. Sci. Technol.* **2014**, *29*, 064006. doi:10.1088/0268-1242/29/6/064006

License and Terms

This is an Open Access article under the terms of the Creative Commons Attribution License (<http://creativecommons.org/licenses/by/2.0>), which permits unrestricted use, distribution, and reproduction in any medium, provided the original work is properly cited.

The license is subject to the *Beilstein Journal of Nanotechnology* terms and conditions: (<http://www.beilstein-journals.org/bjnano>)

The definitive version of this article is the electronic one which can be found at:
doi:10.3762/bjnano.5.226